HHS Public Access

Author manuscript

Org Biomol Chem. Author manuscript; available in PMC 2021 October 13.

Published in final edited form as:

Org Biomol Chem. 2021 March 04; 19(8): 1835–1846. doi:10.1039/d0ob02313b.

Donor Acceptor Fluorophores: Synthesis, Optical Properties, TD-DFT and Cytotoxicity Studies

Zahraa M Essam[a,b,‡], **Guliz Ersoy Ozmen**[a,‡], **Dani Setiawan**[a], **Riri Rizkianty Hamid**[c], **Reda M Abd El-Aal**[b], **Ritu Aneja**[c], **Donald Hamelberg**[a,d], **Maged Henary**[a,d]

[a]Department of Chemistry, Petit Science Center, Georgia State University, 100 Piedmont Avenue SE, Atlanta, Georgia, 30303, United States.

[b]Department of Chemistry, Suez University, Suez, Egypt.

[c]Department of Biology, Petit Science Center, Georgia State University, 100 Piedmont Avenue SE, Atlanta, Georgia, 30303, United States

[d]Center of Diagnostics and Therapeutics, Petit Science Center, Georgia State University, 100 Piedmont Avenue SE, Atlanta, Georgia, 30303, United States.

Abstract

Donor – π – acceptor (D – π – A) fluorophores consisting of a donor unit, a π linker, and an acceptor moiety, attracted attention in the last decade. In this study, we report the synthesis, characterizations, optical properties, TD-DFT, and cytotoxicity studies of 17 near infra-red (NIR) D – π – A analogs which have not been reported so far to the best of our knowledge. These fluorophores have a chloroacrylic acid as the acceptor unit and various donor units such as indole, benzothiazole, benzo[*e*]indole, and quinoline. The fluorophores showed strong absorption in the NIR (700–970 nm) region due to their enhanced intramolecular charge transfer (ICT) between chloroacrylic acid and the donor moieties connected with the Vilsmeier – Haack linker. The emission wavelength maxima of the fluorophores were in between 798–870 nm. Compound **20** with 4- quinoline donor moiety showed an emission wavelength above 1000 nm in the NIR II window. The synthesized fluorophores were characterized by ^{1}H NMR, ^{13}C NMR, and their optical properties were studied. Time dependent density functional theory (TD-DFT) calculations showed that the charge transfer occurs from the donor groups (indole, benzothiazole, benzo[*e*]indole, and quinoline) to the acceptor chloroacrylic acid moiety. Fluorophores with [HOMO] to [LUMO+1] transitions were shown to possess charge separation character. The cytotoxicity of selected fluorophores, **4, 7, 10** and **12** were investigated against breast cancer cell lines and they showed better activity than the anti-cancer agent docetaxel.

‡These authors contributed equally to this work.

Author Contributions

M.H., G.O. and Z.E.; methods development. M.H., D.H., R.A, G.O, D.S., Z.E., R.H.; data acquisition, M.H., G.O., D.S., R.H. and Z.E.; writing-original draft preparation, M.H., D.H., R.A., R.A.E., G.O., D.S., Z.E. and R.H.; writing-review and editing, M.H., D.H. and R.A.; supervision.

Conflicts of interest

Authors declare no conflicts of interest.

†Electronic Supplementary Information (ESI) available: [details of any supplementary information available should be included here]. See DOI: 10.1039/x0xx00000x

Graphical Abstract

We report a series of NIR D-A fluorophores with cyanoacrylic acid acceptor and various donor units. The cytotoxicity of selected fluorophores against triple negative breast cancer cell lines showed stronger activity than anticancer agent docetaxel.

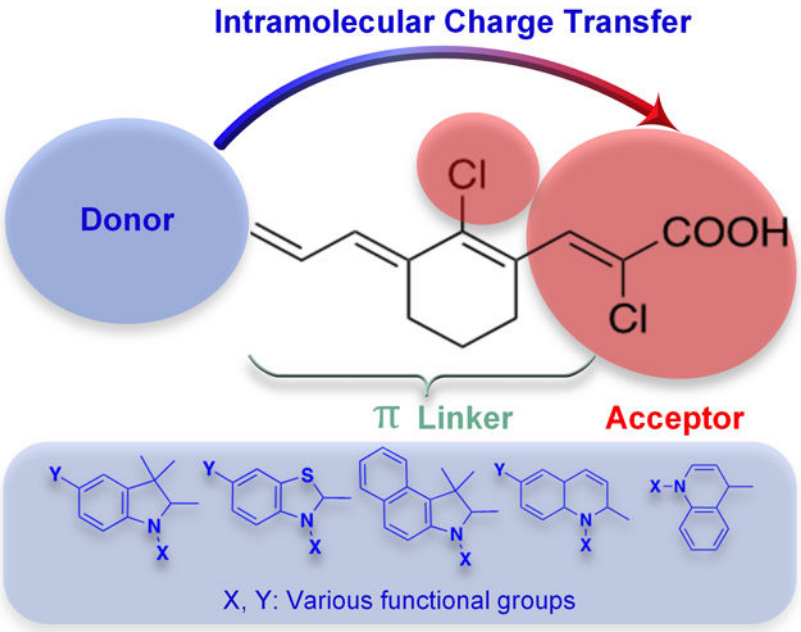

Introduction

Donor– **π** – acceptor (D – **π** – A) fluorophores have attracted attention among researchers in the last decade owing to their push-pull systems[1]. This class of fluorophores has a donor unit and an acceptor moiety at each end, which are connected by a conjugated **π** system. This conjugation enables an intramolecular charge transfer (ICT) and creates the push-pull system[1], yielding a lower energy molecular orbital (MO)[2]. With a combination of strong electron donor and acceptor units at each end of the fluorophore, the fluorescence properties can be altered from ultraviolet-visible (UV-vis) to near infrared (NIR)[1]. The NIR window is essential for bioimaging since photons can penetrate deeper into the tissue, and there is low autofluorescence from biomolecules and tissues[3]. In addition to the bioimaging, NIR D – **π** – A fluorophores find application in various areas such as dye-sensitized solar cells (DSCs)[4], organic light emitting diodes (OLEDs)[5], biosensors[6], and nonlinear optical imaging[7].

Most of the D – π – A fluorophores which were reported so far have emission in UV-vis region[2, 4, 8]. Several studies were performed to synthesize and investigate the optical properties of bathochromic (red) shifted D – π – A fluorophores[1, 9]. In these studies, the effect of various donor and acceptor groups and the effect of chain length of their π system on absorption and fluorescence were investigated. Factors affecting the properties of D – π – A systems are (1) the strength of donor and acceptor units, (2) the length and the composition of the π linker system, and (3) planarization degree of the fluorophore

molecule[2]. These factors may result in decreased energy band gap between donor and acceptor units that contribute to red shift of the emission wavelength maxima[2]. Examples of the various commonly investigated donor and acceptor moieties are presented in Figure 1.

Some examples of donor units are phenyl[10], dimethylamino[2], diphenylamino[2], indoline[4], carbazole[11], and julolidine[2], and examples of common used acceptor moieties are; trifluoromethyl[9], cyanoacetic acid[4], 2-dicyanomethylidene-3- cyano- 4, 5, 5- trimethyl-2, 5-dihydrofuran (TCF)[1], pentafluorosulfonyl[9], thiobarbituric acid[8] and malononitrole[8]. As an example, Kulhanek *et al.* synthesized 4,5-dicyanoimidazole acceptor containing fluorophores by Suzuki-Miyaura cross coupling reaction and investigated the effect of donor groups methoxy and dimethylamino on optical properties which showed the largest red shift for *N,N*- dimethylamino donor group[12]. Additionally, the π linker between donor and acceptor units also contributes to the optoelectronic properties of the fluorophore since it changes the spatial arrangement and electronic structure of the molecules. Therefore, the authors compared styryl and biphenyl linkers attached to the dimethylamino donor unit. Biphenyl linker containing fluorophore showed less fluorescence intensity due to sterically pushing 4,5-dicyanoimidazole unit out of plane[12]. Instead of using an alkene or alkyne as π linker, heteroatomic species can also be used. As an example, Meek *et al.* reported the synthesis of isobenzofuran (IBF) and isothionapthene (ITN) containing donor acceptor fluorophores and IBF containing fluorophores showed red shifted absorption compared to ITN in the NIR region[10]. Another example of the D – π – A fluorophores and its derivatives in NIR region (λ_{em} = 710–800 nm), synthesized by Remond *et al.* using TCF which possess strong electron accepting cyano units[1]. In addition to these examples, it is reported that the planarization of the fluorophore enhances the bathochromic shift by lowering the energy band gap. This was reported by Achelle et al. comparing the donor groups diphenylamino and dimethylamino and the results showed that diphenylamino group disrupts the planarization while dimethylamino does not[2, 13]. There are several other examples of donor acceptor fluorophores reported in recent years[14–19].

To address the need of D – π – A push-pull fluorophores operating in the NIR region, in this study, we designed 17 novel fluorophore scaffolds, which absorb light in the NIR I region. The general structure of the synthesized fluorophores is shown in Figure 2. We synthesized fluorophores with chloroacrylic acid acceptor connected to **π**-conjugated linker such as Vilsmeier- Haack linker with cyclohexene and chlorine atom at the meso carbon and various donor moieties such as indole, benzothiazole, benzo[*e*]indole and quinoline. We investigated the charge transfer between donor and acceptor groups using TD-DFT studies. The selected fluorophores, **4, 7, 10** and **12,** were further investigated for cytotoxicity against triple negative breast cancer (TNBC) cell lines HCC1806, HCC70 and BT-20.

Results and Discussion

We synthesized 17 D – **π** – A fluorophores containing chloroacrylic acid as the acceptor moiety and varying donor units such as; indole, benzothiazole, benzo[*e*]indole and quinoline. The acceptor and donor units are connected by the Vilsmeier Haack linker containing cyclohexene with chloride at the meso carbon to enhance rigidity of the molecule[20]. The chloroacrylic acid, which is both the acceptor and linker unit, was

synthesized and then reacted with the different heterocyclic salts **A-E** to yield the 17 D – **π** – A fluorophores. The TD-DFT studies of fluorophores **4–20** were performed with five different solvents, to optimize their geometries and to investigate the intramolecular charge transfer (ICT) within the molecules. Solvatochromism of selected fluorophores were studied both experimentally and theoretically using TD-DFT. The Natural Transition Orbitals (NTO)[21] for the two highest occupied molecular orbitals (HOMO) and two lowest unoccupied molecular orbitals (LUMO) for each compound corresponding to the $S_0 \rightarrow S_1$ transitions were also calculated and analysed (Supplementary Information Table S6). Cytotoxicity *in vitro* activities of selected fluorophores, **4, 7, 10** and **12**, were performed using triple negative breast cancer (TNBC) cell lines, HCC 1806, HCC 70, and BT-20 by MTT 3- (4,5-dimethylthiazol-2-yl)-2,5-diphenyltetrazolium bromide assay. The cytotoxicity results of selected fluorophores were compared to the anti-cancer agent docetaxel.

Synthesis of D – π – A Fluorophores

The linker unit was synthesized via Vilsmeier Haack formylation. First, dichloromethane (DCM), *N, N*-dimethylformamide (DMF) and phosphoryl chloride ($POCl_3$) were allowed to react, followed by the addition of cyclohexanone (**1**) to yield carbaldehyde (**2**) as outlined below in Scheme 1. Then, the unit containing the acceptor and linker (**3**) was synthesized by reacting carbaldehyde (**2**) and chloroacetic acid under basic conditions (Scheme 1a). Finally, the linker and acceptor unit (**3**) was reacted with heterocyclic salts **A**-**E** (Scheme 1b) under basic condition in ethanol, to yield fluorophores **4–20** as illustrated in Scheme 2.

The indolium (**A**), benzo[*e*]indolium (**C**), 2 and 4 quinolinium (**D, E**) heterocyclic salts were synthesized according to the previously reported procedures by our group[22, 23]. The benzothiazolium (**B**) heterocyclic salts were synthesized according to the reported procedure[24]. After purification of the heterocyclic salts **A-E**, they were allowed to react with the acceptor and linker unit (**3**) for the required time, which was ranged between 1–15 h, for individual heterocyclic salt to yield the desired fluorophores **4–20** which are presented in Scheme 2 with yields between 50–70%. After the reaction completed, they were purified by column chromatography using methanol and DCM (2:1) or by several recrystallizations using minimum amount of methanol to dissolve the fluorophore and precipitating it with ethyl acetate until it is purified. The reaction between quaternary salt moieties **A**-**E** and the π linker and acceptor unit (**3**) proceeded by the condensation under basic condition[25]. The 1H NMR peaks at 6.5 ppm and between 7.0–8.5 ppm (Supplementary Information Figure S1–S35) show the bridge between linker and donor unit indicating the fluorophores were synthesized successfully.

The electron accepting ability of carboxylic acid together with the inductively withdrawing effect of chloride creates a strong electron acceptor unit. The acceptor unit and the electron donating ability of the donor units create a push-pull system and result in absorbance signal in the NIR I region. As shown in Scheme 2, each fluorophore **4–11** have an indole unit where the nitrogen atoms of the heterocycle rings, were functionalized with methyl, ethyl, butyl and ethoxy groups. Fluorophores **12–15** have benzothiazole donor unit that have various length of alkyl chains attached to the heterocycle ring nitrogen atoms. Fluorophores **16** and **17** contain benzo[e]indole heteroatomic donor with N-methyl and N-hexyl groups.

The quinoline containing fluorophores **18–20** have benzyl and methyl functionalized nitrogen atoms.

Optical Studies

The experimental and computed absorbance wavelength maxima (λmax) and molar absorptivity constants (ε) for fluorophores **4–20** are presented in Table 1. For the computed values of λmax, the BLYP functional method, among others, was chosen, since it gives the closest excitation energy when compared to the experimental results (Supplementary Information TableS6). As presented in Table 1, although there is a difference between the experimental and computed absorbances, they are in a good agreement with the experimental results. As an example, for fluorophores with indole donor unit, the absorbance of fluorophore **4** is 780 nm experimentally. Fluorophore **10** with the methoxy group on the indole donor has absorbance experimentally at 810 nm and this difference is also seen for the calculated values as a change from 586 nm to 614 nm. Fluorophore **20** with 4-quinoline has experimental absorbance at 970 nm and its theoretical absorbance is also red shifted at 638 nm. The molar absorption coefficients (ε) of the fluorophores are in the range of 100,000 – 264,600 M-1cm-1. As shown in Table 1, the experimental molar absorptivity constants also show a similar trend with the calculated ones. As an example, the molar absorptivity constant for fluorophores **14** and **15** with benzothiazole donor units have been experimentally found to be 107,000 and 108,320 $M^{-1}cm^{-1}$ and the theoretical values are 108,953 and 107,537 $M^{-1}cm^{-1}$, respectively. The emissions of fluorophores are ranging between 798 nm to 870 nm and fluorophores with 2-quinoline donor moiety showed the largest red shift in emission. Fluorophores **5** and **8** with indole, and **15** with benzothiazole donor unit have the largest Stokes shift values. The highest quantum yields were calculated for fluorophores **13** with benzothiazole and **19** with 2-quinoline donors. The absorption spectra of fluorophores **4–20** are presented in Figure 3. Their absorption wavelength maxima were located between 780–970 nm and fluorophores **18–20** showed significant red shift. The fluorophores showed an emission in NIR with emission wavelength maxima between 798–870 nm. Fluorophore **20** containing 4-quinoline donor has the largest red shift and therefore its fluorescence was out of the range of our equipment which can measure up to 1000 nm. The red-shifted behavior of fluorophore **20** can arise from the planarity of the benzyl ring on the molecule having the strong electron donor benzyl quinoline. Fluorophores **18** and **19** which have 2-quinoline units also show stronger bathochromic shift than the other fluorophores with λ_{em} = 870 nm. Fluorophores containing benzothiazole ring **12–15** have λ = 812 nm. The fluorescence quantum yield of fluorophore **13** was found to be the highest quantum yield (Φ = 0.19) in ethanol. While fluorophore **12** has an ethyl chain, fluorophore **13** has a longer alky chain which resulting in higher quantum efficiency. The benzo[*e*]indole heterocyclic unit substituted fluorophores **16** and **17** have λ_{max} = 822 and 828 nm, respectively. Fluorophore **17** with longer alkyl chain has relatively smaller red shift and quantum efficiency comparable to fluorophore **16**. Fluorophores with indole unit **4–11** have emission wavelength maxima between 801–820 nm. Fluorophores **10** and **11** with methoxy substituted indole show higher bathochromic shift than fluorophores **6–9** which have halogens substituted indole donor. The electron donating ability of methoxy makes indole a stronger donor while bromine and chlorine atoms inductively decrease the electron density

on indole moiety. Fluorophores **4** and **5** with alkyl substituted nitrogen atoms have emission wavelength maxima at 810 and 801 nm, respectively, and showing that longer alkyl chain on nitrogen atom at compound **5** results in smaller red shift. The fluorophores with methoxy substituted indole heterocycles **10** and **11** showed lower molar absorptivity than fluorophores **4** and **5** due to the electron donating nature of the methoxy group introducing electron density back into the system. The large Stokes shifts of fluorophores **4** and **16** indicate that the molecule undergoes a structural change upon excitation.

Solvatochromic Study

The solvatochromic properties of selected fluorophores with different donor units such as; **7** and **8** with indole, **15** with benzothiazole and **17** with benzo[*e*]indole were studied in five solvents; ethanol, methanol, dimethylsulfoxide (DMSO), acetonitrile and DCM. The fluorophores were not soluble in non polar solvents like hexane, toluene and diethyl ether. The absorbance wavelength maxima of these fluorophores were blue shifted for 5 nm in methanol and acetonitrile, while in DMSO and DCM they showed red shift for 5–15 nm (Supplementary Information Table S2). The Stokes Shift (Δ v) and solvent polarizability (Δ *f*) values were used to calculate the slope of Lippert-Mataga equation for these fluorophores[26]. The slopes of these lines, presented in Figure 4, varying between 618–1706 cm^{-1}, are directly proportional to the change in dipole moment upon excitation[27]. Due to the relatively small values of slopes, the dipole moment change is not large, however the slopes for fluorophores **15** and **17** were larger than the slopes of fluorophores **7** and **8** which indicates a larger dipole moment change. This similar behavior of small dipole moment change were also reported with cyanine dyes that have similar backbone structure[28]. In addition to the experimental studies, solvatochromism of the selected fluorophores with addition of **19**, were also studied using TD-DFT (Supplementary Information Table S4). Fluorophore **19** showed low intensity emission peaks experimentally, which may occur due to the competing electron delocalization on the benzene ring of quinoline, therefore it's solvatochromism was studied using TD-DFT[29]. The fluorophores were not soluble in low polarity solvents such as hexane and toluene, and in water the absorbance peaks were broadened. Therefore, solvatochromism of fluorophores in toluene and water were studied using TD-DFT. In toluene fluorophores **7, 8, 15** and **17** showed slightly blue shift and for fluorophore **19** there was 14 nm red shift. In water, the absorbance maxima of all fluorophores were slightly red shifted.

Density Functional Theory Calculations of Fluorophores 4–20

The TD-DFT calculations for the lowest $S_0 \rightarrow S_1$ electronic transition energies of molecule **4–20** with pure DFT functional BLYP give overestimation between 0.39–0.56 eV (MAE 0.49 eV, Supplementary Information Table S6). This behavior is expected from TD-DFT calculations of some classes of chromophores, including cyanines and its derivatives[30–32]. While self-interaction error[33, 34] in pure DFT(approximate GGA functionals) is known to be responsible for general underestimation of charge transfer state energies[35–37], the overestimation in cyanines has been attributed particularly to the differential (non-dynamic) correlation effects in the ground and in the excited states[38, 39]. While the underestimation of charge transfer states can be remedied by the use of larger fraction of Hartree-Fock exchange

mixed within the hybrid DFT functionals[40–43], the overestimation due to the non-dynamic correlation effects can only be remedied by multireference wavefunction methods[44, 45] or ΔSCF-based DFT methods[31, 32]. Hybrid functionals, B3LYP[46–48] and BH&HLYP[49], which approximately contain 25% and 50% of Hartree-Fock exact exchange respectively, have much worse overestimation than the pure density functionals (Supplementary Information, Figure S47). We also tested long range corrected functionals such as

LC-ωHPBE[50], CAM-B3LYP[51] or ωB97XD[52] which also give higher overestimation error. However, despite the quantitative inaccuracies, TD-DFT is able to reproduce the trend in energy perfectly well, albeit qualitatively. It can be seen from the relative comparison of $S_0 \rightarrow S_1$ excitation energies among the fluorophores (Figures 3 and 5). Among the fluorophores with indole donor units, the lowest $S_0 \rightarrow S_1$ excitation energies belongs to fluorophores **11** and **10** respectively, while fluorophores **4–9** have similar, higher excitation energies. For benzothiazoles (**12–15**) and benzo[*e*]indoles (**16–17**), each of the molecules shows similar $S_0 \rightarrow S_1$ excitation energy levels respectively. For quinolines (**18–20**) the TD-DFT calculations also predict the trend in accurate manner, that the $S_0 \rightarrow S_1$ excitation energies for **20 < 19 < 18**. The highest experimental absorption peak for all compounds are due to the lowest energy, $S_0 \rightarrow S_1$ excitation (TD-DFT calculations, Figure 5), each corresponds to [HOMO] to [LUMO] electronic transition. These [HOMO] → [LUMO] transition, all have charge transfer character from donor to chloroacrylic acid acceptor (Supplementary Information Figure S48–S64). Both chlorine atoms in the chloroacrylic and at meso carbon of the Vilsmeier-Haack linker seems to play a role as one electron withdrawing moiety. For indoles, the higher energy $S_0 \rightarrow S_2$ excitations correspond to [HOMO-1] → [LUMO], while for benzothiazoles, benzo[*e*]indoles, and quinolines this state corresponds to [HOMO] → [LUMO+1] transitions. The $S_0 \rightarrow S_2$ excitations are found to be excited states with the second highest oscillator strength (except for benzo[*e*]indoles and quinoline **18** and **20**).

In benzo[*e*]indoles [HOMO-1] → [LUMO] corresponds to the higher energy $S_0 \rightarrow S_3$ state, with the $S_0 \rightarrow S_2$ excitation states become a hidden state (Figure 5c). As with the [HOMO] → [LUMO] transition, the [HOMO-1] → [LUMO] also corresponds to charge transfer transition from donor to acceptor region (Figure 5 and 6). Interestingly, for [HOMO] → [LUMO+1] transition, it represents some kind of “charge separation” character in which electrons could undergo localization onto both donor and acceptor ends of the molecule, leaving a lesser electron density in the linker region resulting in a more polarized molecule (Figure 6). In fluorophores with quinoline donor however, while the $S_0 \rightarrow S_2$ state ([HOMO] →[LUMO+1]) in **18** and **19** has considerable oscillator strength, fluorophore **20** has instead a very low oscillator strength (f = 0.02, Figure 5d) that this state can be considered as a hidden excited state. This could be attributed to the fact that the phenyl group in fluorophore **20** is directly in opposite of the D-**π**-A molecular plane, thus may disturbs the electronic structure of the quinoline moiety while for fluorophore **19** the phenyl is sideways. For fluorophore **18**, the disturbance could be due to the presence of electron withdrawing carboxylic acid group at the donor quinoline moiety.

Photostability

Photodegradation is an important property of dyes for their practical applications. The fluorophores should be stable upon excitation for a certain time. Fluorophores **4, 7, 11** and **13** were selected to study the photostability of dyes. The studies were performed according to our published method[26]. The fluorophores were dissolved in methanol by sonicating and then diluted to give absorbance values 0.6. The solutions were divided to two parts, one kept in dark (Supplementary Information Figure S46) and the other kept in front of 15 W UV lamp (Figure 7). On the other hand, fluorophore **13** showed 100% photofading after 3 days. Fluorophores **4, 7** and **11** showed higher stability than ICG which is an FDA approved probe for bioimaging.

Fluorophores **4, 7, 10** and **12** were selected based on their hydrophilicity and molar absorptivity constants to further investigate their cytotoxicity (IC_{50}) against breast cancer. Three different triple negative breast cancer (TNBC) cell lines HCC 1806, HCC 70 and BT-20 were used for the cytotoxicity studies. The IC_{50} of the fluorophores are compared with the IC_{50} of the common anti-cancer drug docetaxel.

Evaluation of Anti-Proliferative Activity of TNBC Cell Lines

Evaluation of the cytotoxic activity of 4 out of 17 novel D – π – A fluorophore analogs of **4, 7, 10, 12** compared to docetaxel, a common chemotherapy drug used for TNBC was done using the MTT assay. Fluorophore analogs **4, 7, 10, 12**, and docetaxel showed IC_{50} values of 0.717, 0.459, 0.402, 0.528 and 50.9 μM, respectively in HCC1806. Similarly, fluorophore analogs **4, 7, 10, 12**, and docetaxel showed IC_{50} values of 0.940, 0.404, 0.807, 1.29, 35.6 μM in HCC70 and 1.47, 0.780, 1.35, 4.42, 2.41 μM in BT-20 correspondingly as Table 2. IC_{50} values of TNBC cell lines against fluorophores **4, 7, 10, 12** and docetaxel shown in Table 2. Figure 8 displays the most potent fluorophore analogs which exhibited IC_{50} below 5 μM in TNBCs compared to docetaxel (Figure 8e). The IC_{50} values in bar graph format with calculated standard deviation between batches of the four fluorophore analogs and docetaxel are displayed in Figure 9 (a and b). As evident from the in-vitro cell proliferation data, fluorophore analogs **4, 7** and **10** with indole unit with nitrogen atoms are more active compared to fluorophore **12** with benzothiazole unit suggesting attenuated biological activity with structural modification of benzothiazole.

Along the same lines, bromine at position 5 of indole unit with an ethyl group on the nitrogen atoms significantly improves the activity as evident upon comparing fluorophore **4** and **7**. Other molecular modifications, including methoxy group on fluorophore **10** slightly improved the biological response but not to the same extent as fluorophore **7**, which also showed the highest molar absorptivity constant in optical studies (Table 1). The more hydrophilic fluorophores with larger stoke shift show better anticancer profiles as seen from the IC_{50} values. The relative efficiency of the fluorophore analogs cannot be correlated entirely to the Stokes Shift, but the most active fluorophore has a large Stokes Shift of 20 nm with smaller stoke shift displaying lower potency. However, to fully understand the anticancer activity of the novel fluorophores, further in-vitro studies comparing the treatment of TNBC cell lines and normal mammary epithelial cells are warranted for the various classes of D – π – A fluorophores **4–20.**

Conclusions

In this work we synthesized 17 D – π – A fluorophores with chloroacrylic acid acceptor and five various types of donor moieties with Vilsmeier- Haack linker. The linker and acceptor were synthesized first and then reacted with heterocyclic salts to yield the desired fluorophores **4–20**. The effect of various type of donors on the fluorophores have been investigated by optical properties and TD-DFT studies to determine the charge transfer between donor and acceptor and their geometries. The synthesized fluorophores have absorption and emission in NIR above 700 nm. Fluorophore **20** containing a quinoline unit showed the highest bathochromic (red) shift. The attached benzyl ring of fluorophore **20** makes the structure more planar and conjugated, promoting ICT. Fluorophores **18** and **19** were also red shifted due to their highly rigid and conjugated systems. For fluorophores **4–11** with indole donor unit, the red shifted behaviour observed with the 5-methoxy substitution rather than halogens due to the electron donating ability of methoxy group. Benzothiazole donor unit containing fluorophores **12–15** showed similar emission wavelength with the indole unit but higher quantum yields were found. Fluorophores **16** and **17** that has benzo[*e*]indole donor possess high quantum efficiencies and compound **16** significantly showed larger Stokes shift which is due to the larger conformation change of the molecule. Addition of longer chain to this donor unit as seen in compound **17** and resulted with less red shifted emission. The solvatochromic studies of selected four fluorophores **7, 8, 15** and **17** showed 5 nm blue shift in methanol and acetonitrile, and 5–15 nm red shift in DMSO and DCM absorption wavelength peaks. The Lippert-Mataga plot of selected fluorophores showed presence of ICT and relatively small Stokes shifts. TD-DFT calculation showed that lowest energy excitations for fluorophores **4–20** is due to $S_0 \rightarrow S_1$ electronic state excitation which dominantly corresponds to [HOMO] → [LUMO] transition (Figure 5). From natural transition orbital analysis, the electronic transition from [HOMO] → [LUMO] itself, is characterized as a charge transfer excitation (Figure 6). Higher excitations (i.e. the second lowest energy excitations) may correspond to either [HOMO-1] → [LUMO] transition (another charge transfer type excitation) found for fluorophores containing indole **4–11** and benzothiazoles **13** and **15** or [HOMO] → [LUMO+1] transition, which results in charge separation like characteristic for fluorophores with donor groups benzothiazole **14**, benzo[*e*]indole **16** and **17**, and quinolines **18–20**. The cytotoxicity results of fluorophores **4, 7, 10** and **12** suggest that fluorophore analogs have a better activity against TNBC cell lines when compared to docetaxel under the same conditions. Specifically, fluorophore **7** with bromine substituent showed strong cytotoxicity against all cell lines. For future studies, a full cytotoxicity studies of fluorophores **4–20** will be investigated for healthy and TNBC cell lines.

Supplementary Material

Refer to Web version on PubMed Central for supplementary material.

Acknowledgements

M.H. would like to thank the Egyptian Cultural and Educational Bureau for the Postdoctoral Fellow ZE, the Georgia State University Brains and Behavior Seed Grant, the Atlanta Clinical and Translational Science Institute

Healthcare Innovation Seed Grant, and the Georgia Research Alliance Ventures Phase 1 Grant for the support. The computational work in D.H. research group was supported in part by National Science Foundation MCB-2018144.

Notes and references

1. Rémond M; Zheng Z; Jeanneau E; Andraud C; Bretonnière Y; Redon S, 4,5,5-Trimethyl-2,5-dihydrofuran-Based Electron-Withdrawing Groups for NIR-Emitting Push–Pull Dipolar Fluorophores. The Journal of Organic Chemistry 2019, 84 (16), 9965–9974. [PubMed: 31319662]
2. Bureš F, Fundamental aspects of property tuning in push–pull molecules. RSC Advances 2014, 4 (102), 58826–58851.
3. Owens EA; Henary M; El Fakhri G; Choi HS, Tissue-Specific Near-Infrared Fluorescence Imaging. Accounts of chemical research 2016, 49 (9), 1731–1740. [PubMed: 27564418]
4. Yang J; Ganesan P; Teuscher J; Moehl T; Kim YJ; Yi C; Comte P; Pei K; Holcombe TW; Nazeeruddin MK; Hua J; Zakeeruddin SM; Tian H; Grätzel M, Influence of the Donor Size in D −π–A Organic Dyes for Dye-Sensitized Solar Cells. Journal of the American Chemical Society 2014, 136 (15), 5722–5730. [PubMed: 24655036]
5. Zhao B; Xie G; Wang H; Han C; Xu H, Simply Structured Near-Infrared Emitters with a Multicyano Linear Acceptor for Solution-Processed Organic Light-Emitting Diodes. Chemistry – A European Journal 2019, 25 (4), 1010–1017.
6. Zhang Q; Zhang J; Zuo H; Wang C; Shen Y, A novel colorimetric and fluorescent sensor for cyanide anions detection based on triphenylamine and benzothiadiazole. Tetrahedron 2016, 72 (9), 1244–1248.
7. Cvejn D; Achelle S; Pytela O; Malval J-P; Spangenberg A; Cabon N; Bureš F; Robin-le Guen F, Tripodal molecules with triphenylamine core, diazine peripheral groups and extended π-conjugated linkers. Dyes and Pigments 2016, 124, 101–109.
8. Manuela M; Raposo M; Herbivo C; Hugues V; Clermont G; Castro MCR; Comel A; Blanchard-Desce M, Synthesis, Fluorescence, and Two-Photon Absorption Properties of Push–Pull 5-Arylthieno[3,2-b]thiophene Derivatives. European Journal of Organic Chemistry 2016, 2016 (31), 5263–5273.
9. Gautam P; Yu CP; Zhang G; Hillier VE; Chan JMW, Pulling with the Pentafluorosulfanyl Acceptor in Push–Pull Dyes. The Journal of Organic Chemistry 2017, 82 (20), 11008–11020. [PubMed: 28945090]
10. Meek ST; Nesterov EE; Swager TM, Near-Infrared Fluorophores Containing Benzo[c]heterocycle Subunits. Organic Letters 2008, 10 (14), 2991–2993. [PubMed: 18563902]
11. Guo L; Wong MS, Multiphoton Excited Fluorescent Materials for Frequency Upconversion Emission and Fluorescent Probes. Advanced Materials 2014, 26 (31), 5400–5428. [PubMed: 24981591]
12. Kulhánek J; Bureš F; Pytela O; Mikysek T; Ludvík J; Růžička A, Push-pull molecules with a systematically extended π-conjugated system featuring 4,5-dicyanoimidazole. Dyes and Pigments 2010, 85 (1), 57–65.
13. Achelle S; Barsella A; Caro B; Robin-le Guen F, Donor–linker–acceptor (D–π–A) diazine chromophores with extended π-conjugated cores: synthesis, photophysical and second order nonlinear optical properties. RSC Advances 2015, 5 (49), 39218–39227.
14. Zhou H; Huang Q; Liu X; Xu D; Zhang W; Fu S; Feng X; Zhang Z, Phenothiazine and diphenylsulfone-based donor–acceptor π-systems exhibiting remarkable mechanofluorochromism. Dyes and Pigments 2021, 184, 108868.
15. Verbitskiy EV; Achelle S; Bureš F; le Poul P; Barsella A; Kvashnin YA; Rusinov GL; Guen F. R.-l.; Chupakhin ON; Charushin VN, Synthesis, photophysical and nonlinear optical properties of [1,2,5]oxadiazolo[3,4-b]pyrazine-based linear push-pull systems. Journal of Photochemistry and Photobiology A: Chemistry 2021, 404, 112900.
16. Noirbent G; Pigot C; Bui T-T; Péralta S; Nechab M; Gigmes D; Dumur F, Synthesis, optical and electrochemical properties of a series of push-pull dyes based on the 2-(3-cyano-4,5,5-trimethylfuran-2(5H)-ylidene)malononitrile (TCF) acceptor. Dyes and Pigments 2021, 184, 108807.

17. Zheng Z; Liu H; Zhai S; Zhang H; Shan G; Kwok RTK; Ma C; Sung HHY; Williams ID; Lam JWY; Wong KS; Hu X; Tang BZ, Highly efficient singlet oxygen generation, two-photon photodynamic therapy and melanoma ablation by rationally designed mitochondria-specific near-infrared AIEgens. Chemical Science 2020, 11 (9), 2494–2503. [PubMed: 34084415]
18. Akchurin IO; Yakhutina AI; Bochkov AY; Solovjova NP; Traven VF, Synthesis of novel push-pull fluorescent dyes – 7-(diethylamino)furo[3,2-c]coumarin and 7-(diethylamino)thieno[3,2-c]coumarin derivatives. Heterocyclic Communications 2018, 24 (2), 85–91.
19. Li L; Xu Y; Chen Y; Zheng J; Zhang J; Li R; Wan H; Yin J; Yuan Z; Chen H, A family of push-pull bio-probes for tracking lipid droplets in living cells with the detection of heterogeneity and polarity. Analytica Chimica Acta 2020, 1096, 166–173. [PubMed: 31883583]
20. Mojzych M; Henary M, Synthesis of Cyanine Dyes. In Heterocyclic Polymethine Dyes: Synthesis, Properties and Applications, Strekowski L, Ed. Springer Berlin Heidelberg: Berlin, Heidelberg, 2008; pp 1–9.
21. Martin RL, Natural transition orbitals. The Journal of Chemical Physics 2003, 118 (11), 4775–4777.
22. Owens EA; Hyun H; Tawney JG; Choi HS; Henary M, Correlating Molecular Character of NIR Imaging Agents with Tissue-Specific Uptake. Journal of Medicinal Chemistry 2015, 58 (10), 4348–4356. [PubMed: 25923454]
23. Basnet K; Fatemipouya T; St. Lorenz A; Nguyen M; Taratula O; Henary M; Grant KB, Single photon DNA photocleavage at 830 nm by quinoline dicarbocyanine dyes. Chemical Communications 2019, 55 (84), 12667–12670. [PubMed: 31584046]
24. Kuramoto N; Natsukawa K; Asao K, Synthesis and characterization of deep-coloured squarylium dyes for laser optical recording media. Dyes and Pigments 1989, 11 (1), 21–35.
25. Levitz A; Marmarchi F; Henary M, Introduction of various substitutions to the methine bridge of heptamethine cyanine dyes Via substituted dianil linkers. Photochemical & Photobiological Sciences 2018, 17 (10), 1409–1416. [PubMed: 30234861]
26. Lippert E, Dipolmoment und Elektronenstruktur von angeregten Molekülen. Zeitschrift für Naturforschung A 1955, 10 (7), 541–545.
27. Seintis K; Agathangelou D; Cvejn D; Almonasy N; Bureš F; Giannetas V; Fakis M, Femtosecond to nanosecond studies of octupolar molecules and their quadrupolar and dipolar analogues. Physical Chemistry Chemical Physics 2017, 19 (25), 16485–16497. [PubMed: 28608877]
28. Berezin MY; Lee H; Akers W; Achilefu S, Near Infrared Dyes as Lifetime Solvatochromic Probes for Micropolarity Measurements of Biological Systems. Biophysical Journal 2007, 93 (8), 2892–2899. [PubMed: 17573433]
29. Zalukaev LP; Vorob'eva RP, An intramolecular charge-transfer complex in hydrogenated quinolines. Chemistry of Heterocyclic Compounds 1970, 4 (2), 218–220.
30. Le Guennic B; Jacquemin D, Taking up the cyanine challenge with quantum tools. Accounts of chemical research 2015, 48 (3), 530–537. [PubMed: 25710687]
31. Filatov M; Huix-Rotllant M, Assessment of density functional theory based ΔSCF (self-consistent field) and linear response methods for longest wavelength excited states of extended **π**-conjugated molecular systems. The Journal of Chemical Physics 2014, 141 (2), 024112.
32. Kowalczyk T; Yost SR; Voorhis TV, Assessment of the ΔSCF density functional theory approach for electronic excitations in organic dyes. The Journal of chemical physics 2011, 134 (5), 054128.
33. Zhang Y; Yang W, A challenge for density functionals: Self-interaction error increases for systems with a noninteger number of electrons. The Journal of chemical physics 1998, 109 (7), 2604–2608.
34. Bao JL; Gagliardi L; Truhlar DG, Self-interaction error in density functional theory: An appraisal. The journal of physical chemistry letters 2018, 9 (9), 2353–2358. [PubMed: 29624392]
35. Dreuw A; Weisman JL; Head-Gordon M, Long-range charge-transfer excited states in time-dependent density functional theory require non-local exchange. The Journal of chemical physics 2003, 119 (6), 2943–2946.
36. Dreuw A; Head-Gordon M, Single-reference ab initio methods for the calculation of excited states of large molecules. Chemical reviews 2005, 105 (11), 4009–4037. [PubMed: 16277369]
37. Kümmel S, Charge-Transfer Excitations: A Challenge for Time-Dependent Density Functional Theory That Has Been Met. Advanced Energy Materials 2017, 7 (16), 1700440.

38. Grimme S; Neese F, Double-hybrid density functional theory for excited electronic states of molecules. The Journal of chemical physics 2007, 127 (15), 154116.
39. Moore B; Autschbach J, Longest-wavelength electronic excitations of linear cyanines: the role of electron delocalization and of approximations in time-dependent density functional theory. Journal of chemical theory and computation 2013, 9 (11), 4991–5003. [PubMed: 26583416]
40. Cremer D, Density functional theory: coverage of dynamic and non-dynamic electron correlation effects. Molecular Physics 2001, 99 (23), 1899–1940.
41. Setiawan D; Kazaryan A; Martoprawiro MA; Filatov M, A first principles study of fluorescence quenching in rhodamine B dimers: how can quenching occur in dimeric species? Physical Chemistry Chemical Physics 2010, 12 (37), 11238–11244. [PubMed: 20676414]
42. Bernard YA; Shao Y; Krylov AI, General formulation of spin-flip time-dependent density functional theory using non-collinear kernels: Theory, implementation, and benchmarks. The Journal of chemical physics 2012, 136 (20), 204103.
43. Huix-Rotllant M; Filatov M; Gozem S; Schapiro I; Olivucci M; Ferré, N., Assessment of density functional theory for describing the correlation effects on the ground and excited state potential energy surfaces of a retinal chromophore model. Journal of chemical theory and computation 2013, 9 (9), 3917–3932. [PubMed: 26592387]
44. Goerigk L; Grimme S, Assessment of TD-DFT methods and of various spin scaled CIS (D) and CC2 versions for the treatment of low-lying valence excitations of large organic dyes. The Journal of Chemical Physics 2010, 132 (18), 184103.
45. Loos P-F; Scemama A; Jacquemin D, The Quest For Highly Accurate Excitation Energies: A Computational Perspective. The Journal of Physical Chemistry Letters 2020, 11 (6), 2374–2383. [PubMed: 32125872]
46. Lee C; Yang W; Parr RG, Development of the Colle-Salvetti correlation-energy formula into a functional of the electron density. Physical Review B 1988, 37 (2), 785–789.
47. Becke AD, Density-functional thermochemistry. I. The effect of the exchange-only gradient correction. The Journal of chemical physics 1992, 96 (3), 2155–2160.
48. Stephens PJ; Devlin FJ; Chabalowski CF; Frisch MJ, Ab initio calculation of vibrational absorption and circular dichroism spectra using density functional force fields. The Journal of physical chemistry 1994, 98 (45), 11623–11627.
49. Becke AD, A new mixing of Hartree–Fock and local density-functional theories. The Journal of chemical physics 1993, 98 (2), 1372–1377.
50. Henderson TM; Izmaylov AF; Scalmani G; Scuseria GE, Can short-range hybrids describe long-range-dependent properties? The Journal of chemical physics 2009, 131 (4), 044108.
51. Yanai T; Tew DP; Handy NC, A new hybrid exchange–correlation functional using the Coulomb-attenuating method (CAM-B3LYP). Chemical physics letters 2004, 393 (1–3), 51–57.
52. Chai J-D; Head-Gordon M, Systematic optimization of long-range corrected hybrid density functionals. The Journal of Chemical Physics 2008, 128 (8), 084106.

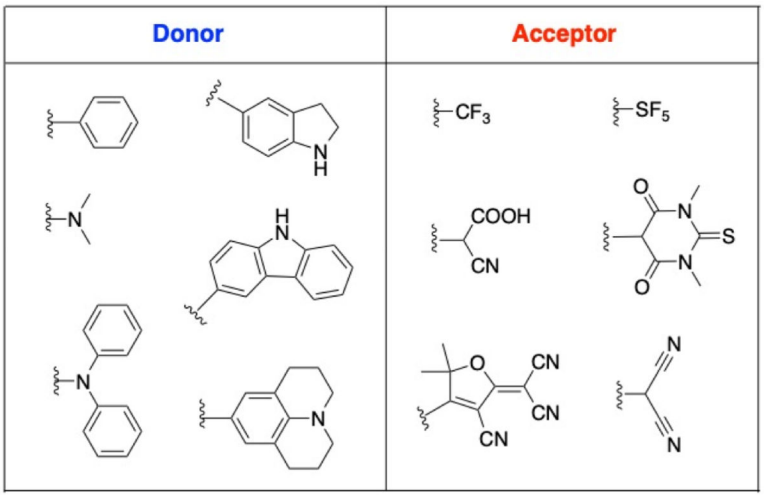

Figure 1.
Various donor and acceptor units investigated for the synthesis of D – π – A fluorophores.

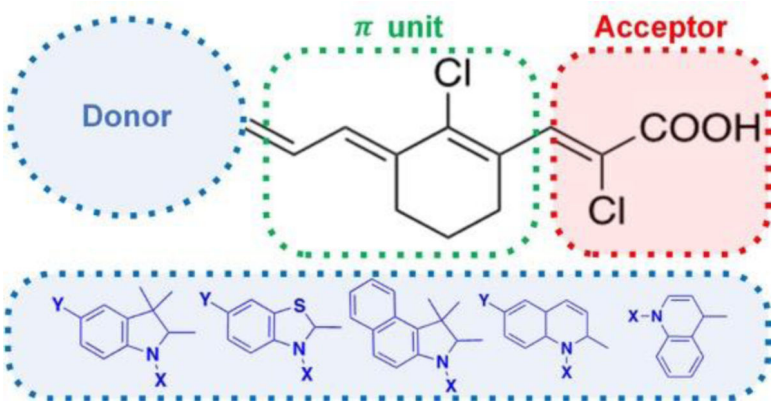

Figure 2.
General structure of the synthesized D – π – A fluorophores **4–20**.

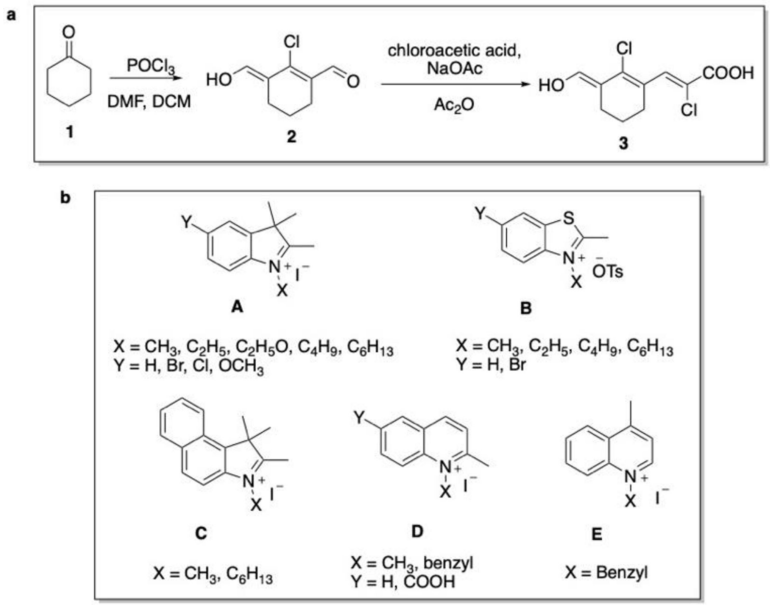

Scheme 1.

a. Synthesis of acceptor and **π** linker unit **3**, b. Various heterocyclic salts (**A**-**E**) which used as donor units.

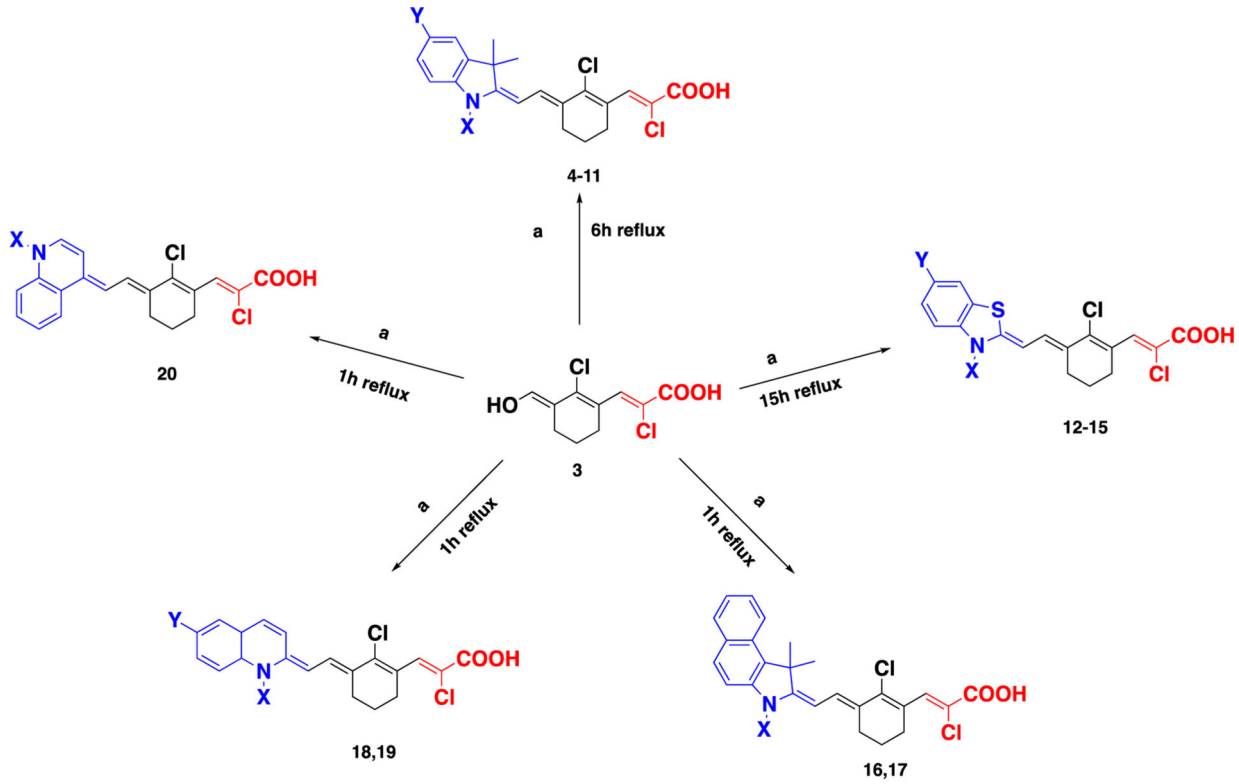

a = NEt_3 and ethanol**, 4:** X = CH_3; Y = H, **5:** X = C_4H_9; Y=H, **6:** X = CH_3; Y = Br, **7:** X = C_2H_5,; Y = Br, **8:** X = C_2H_5,; Y = Cl, **9:** X = C_2H_5O; Y = Br, **10:** X = CH_3; Y = OMe, **11:** X = C_4H_9; Y = OMe, **12:** X = C_2H_5,; Y = H**, 13:** X = C_6H_{13}; Y = H, **14:** X = CH_3; Y = Br, **15:** X = C_4H_{10}; Y = H, **16:** X = CH_3, **17:** X = C_6H_{13}, **18:** X = CH_3; Y = COOH, **19:** X = benzyl; Y = H, **20:** X = benzyl, Y = H

Scheme 2.

General synthesis of D – π – A fluorophores **4–20**.

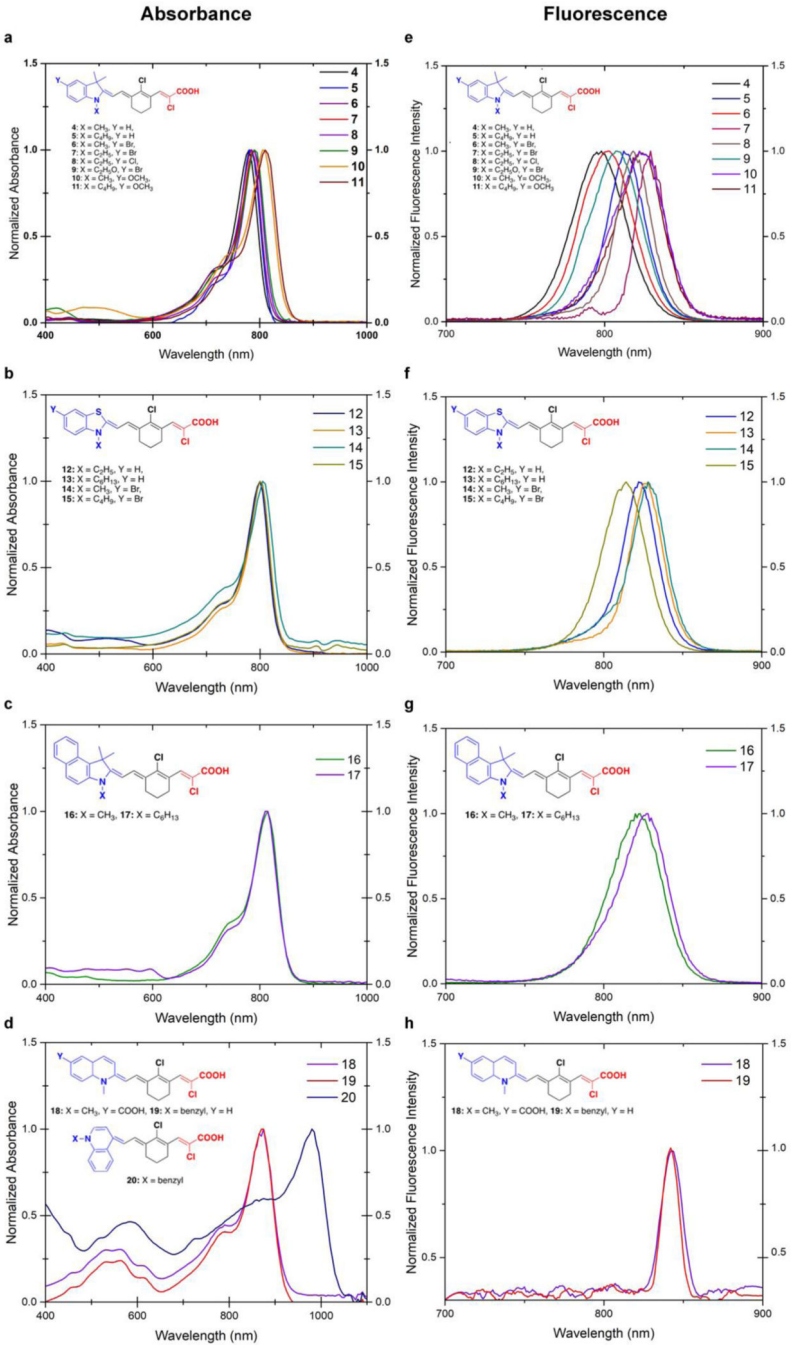

Figure 3.

Absorption and fluorescence spectra of fluorophores **4–20**, a) absorption spectra of fluorophores **4–11**, b) absorption spectra of fluorophores **12–15**, c) absorption spectra of fluorophores **16** and **17**, d) absorption spectra of fluorophores **18–20**, e) fluorescence spectra of fluorophores **4–11**, f) emission spectra of fluorophores **12–15**, g) emission spectra of fluorophores **16** and **17**, h) emission spectra of fluorophores **18** and **19**.

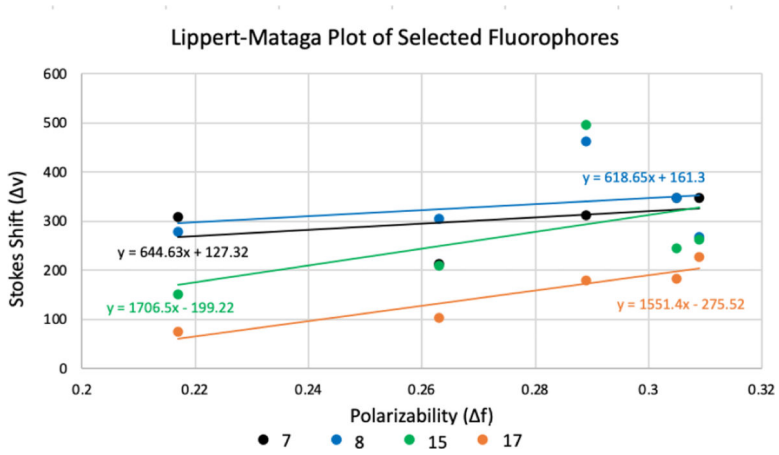

Figure 4.

Lippert-Mataga plots of selected fluorophores **7, 8, 15** and **17**.

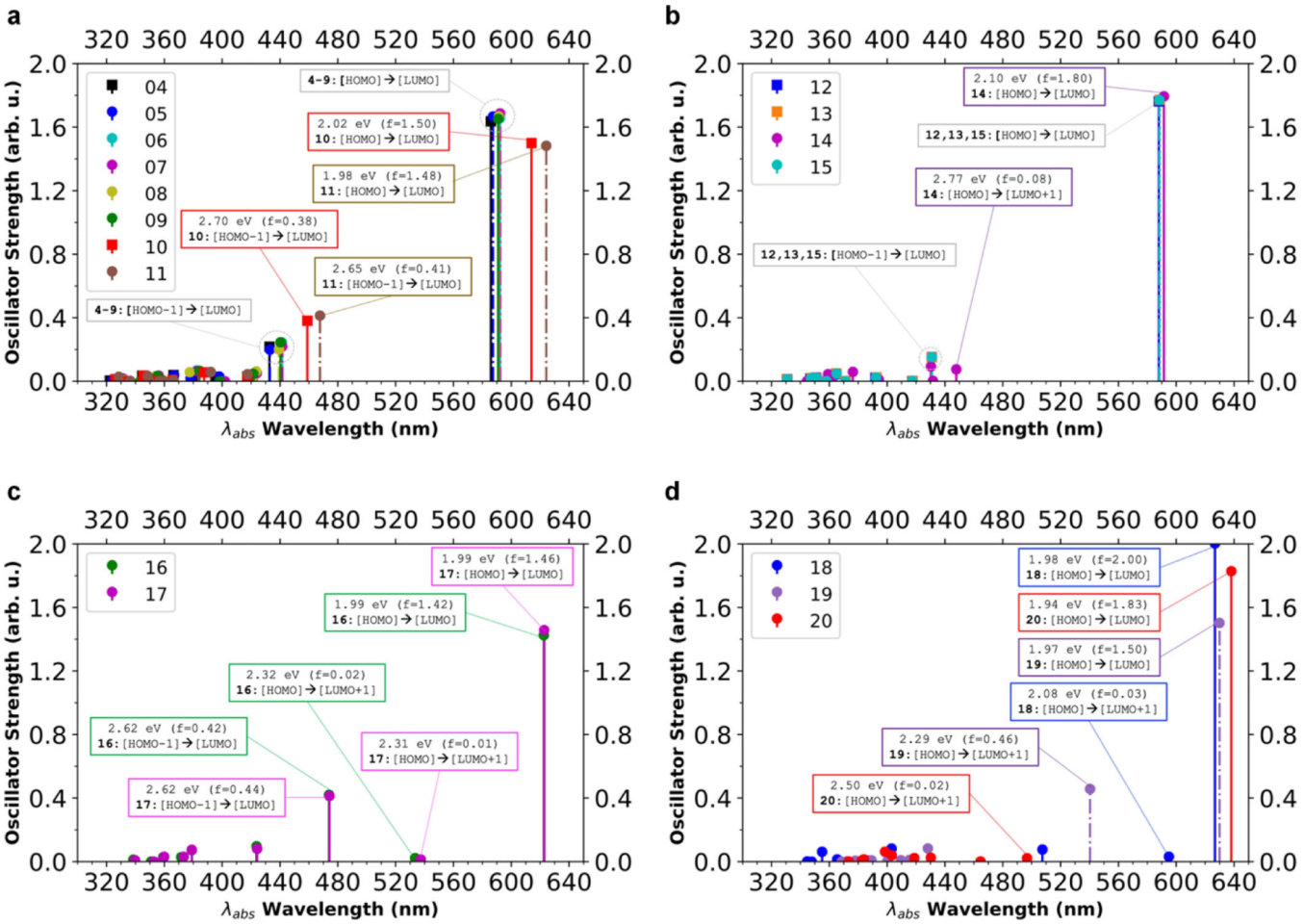

Figure 5.

Computational TD-DFT results for a) indoles, b) benzothiazoles, c) benzo[e]indoles, d) quinolines. Calculated spectra are shown in terms of oscillator strength. For each compound, the highest absorption peaks correspond to a HOMO to LUMO transition.

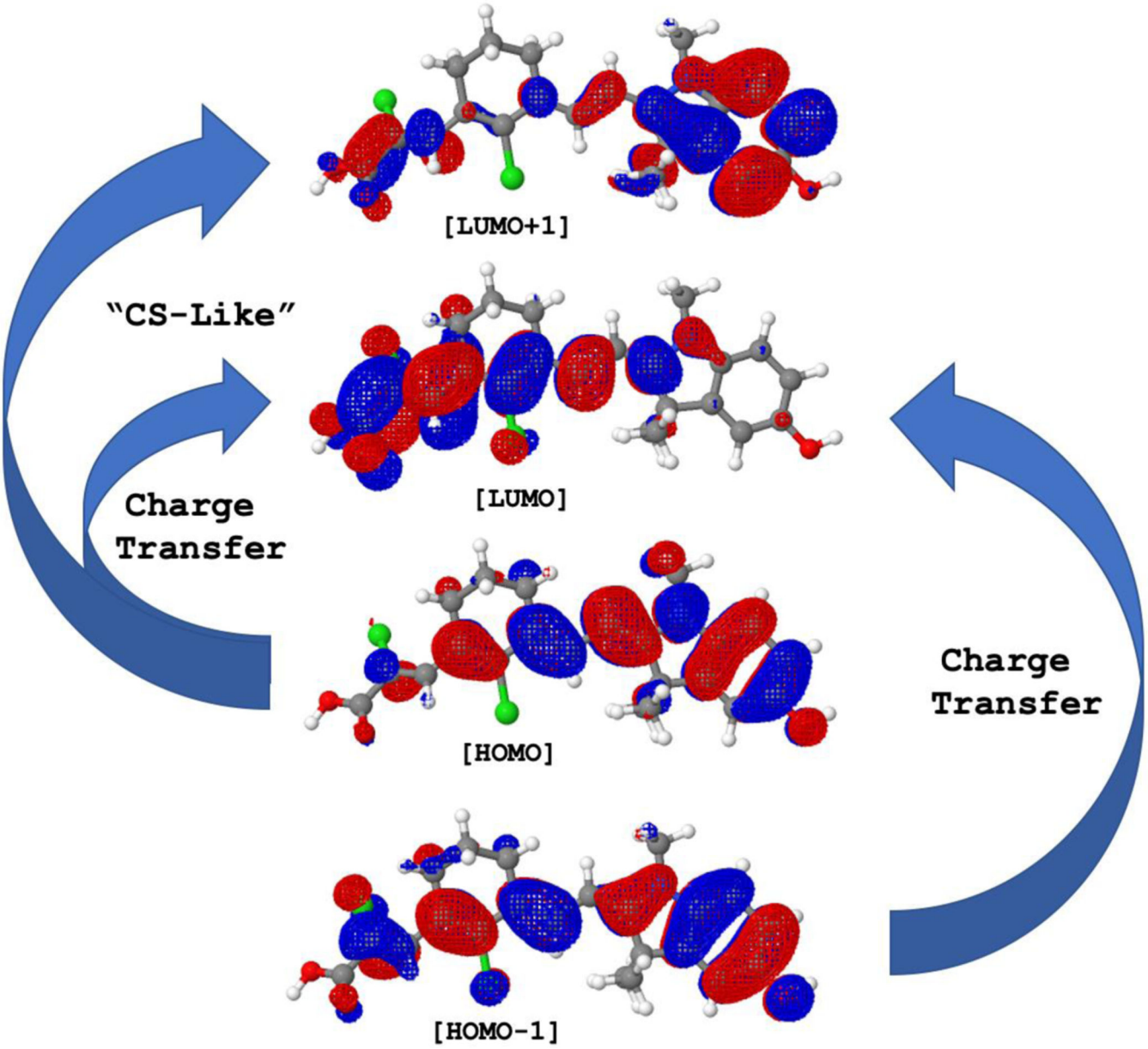

Figure 6.

Charge transfer excitations correspond to either [HOMO] → [LUMO] or [HOMO-1] → [LUMO] electronic transitions shown for fluorophore **10**. The [HOMO] → [LUMO+1] give a charge-separated-like ("CS-like") character. The natural orbitals were calculated at HF/6–311G level of theory.

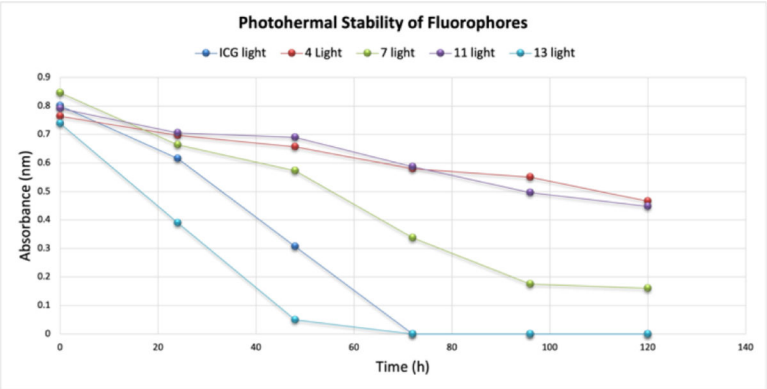

Figure 7.
Photostability test of fluorophores **4, 7, 11** and **13**.

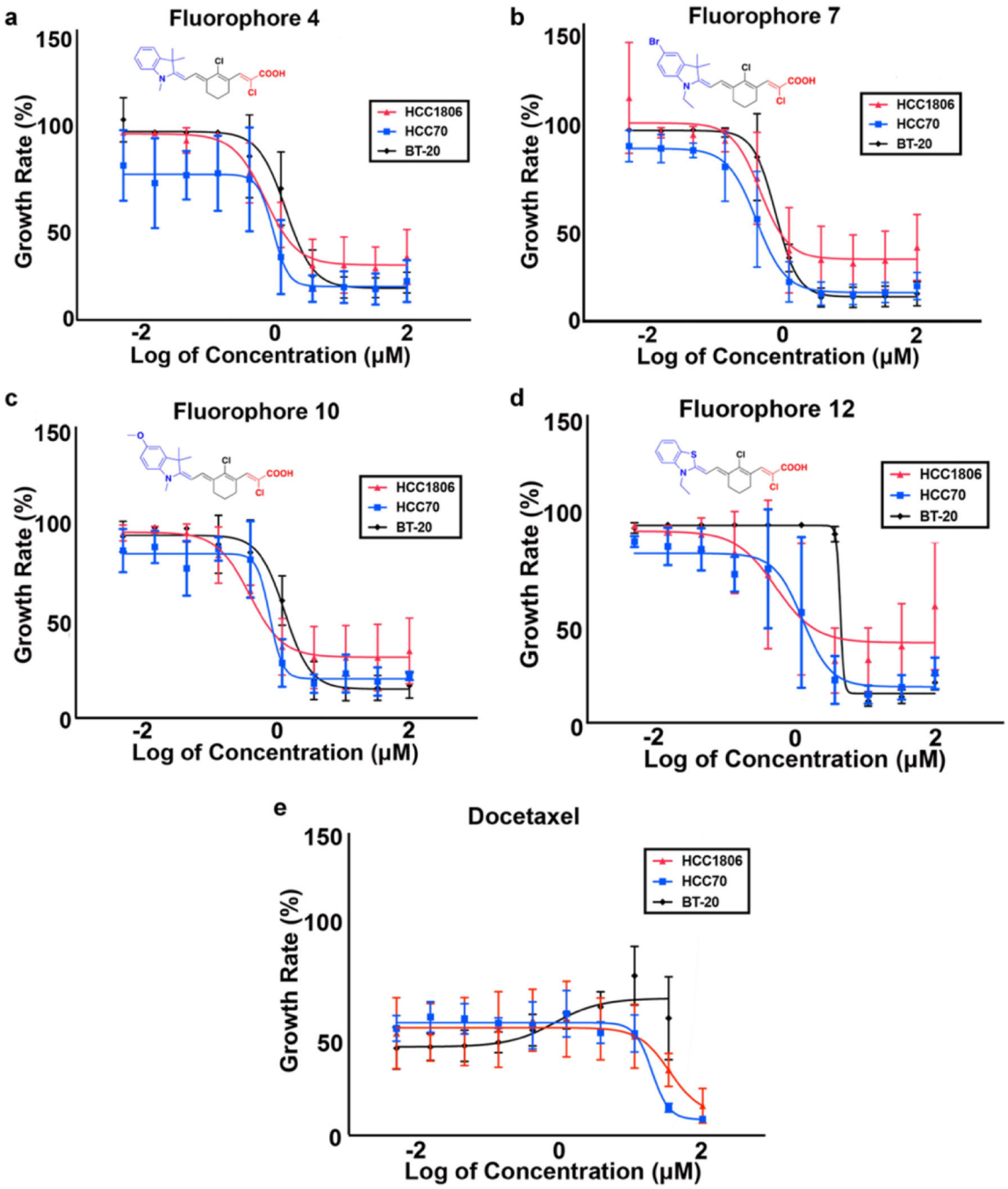

Figure 8.

TNBC cells were treated with increasing concentration of fluorophore analogs and docetaxel, to measure the percentage of cell proliferation using MTT assay.

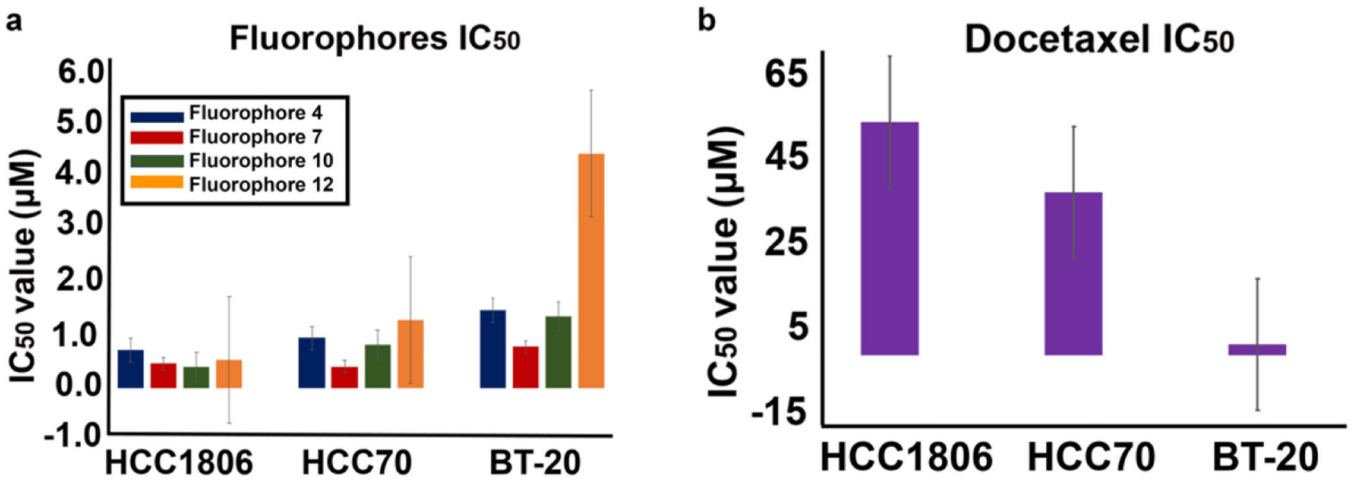

Figure 9.

Inhibitory concentration at 50% (IC50) values of breast cancer cell lines against fluorophores **4, 7, 10, 12** (A) in comparison to docetaxel (B).

Table 1.

Optical properties of fluorophores **4–20**.

Fluorophore	λ_{abs} (nm)		λ_{em} (nm)	Stokes Shift (cm^{-1})	ε (10^3 cm^{-1} M^{-1})		Φ (%)
	Exp	Cal			Exp	Cal	
4	780	586	798	289	111	99	10
5	785	587	813	439	112	101	11
6	784	592	804	317	124	100	8
7	790	592	810	313	265	102	12
8	790	591	820	463	200	101	7
9	790	591	811	328	162	100	9
10	810	614	825	224	106	91	8
11	815	624	826	163	107	90	10
12	800	588	812	185	105	107	13
13	800	589	812	185	104	108	19
14	805	592	830	374	107	109	12
15	800	588	833	495	108	108	11
16	815	623	824	134	112	87	16
17	810	623	822	180	107	89	15
18	860	627	870	134	107	122	16
19	860	630	870	134	100	91	17
20	970	638	-	-	100	111	-

a = fluorescence quantum yield, given absorption and emission maxima were measured in ethanol using ICG as a reference (Φ_{ICG} = 0.13[25]).

Table 2.

IC_{50} values of TNBC cell lines against fluorophores **4, 7, 10**, **12**and docetaxel

Cell Lines	IC_{50} of Fluorophores (μM)				IC_{50} of Docetaxel (μM)
	4	7	10	12	
HCC 1806	0.717	0.459	0.402	0.528	50.9
HCC 70	0.940	0.404	0.807	1.290	35.6
BT-20	1.470	0.780	1.350	4.420	2.41